Contents lists available at ScienceDirect

EBioMedicine

The metabolic footprint during adipocyte commitment highlights ceramide modulation as an adequate approach for obesity treatment

Weilong Hou[a,1], Qiang Chen[a,1], Haitao Wang[a,b,c,d], Pengxiang Qiu[a], Xueying Lyu[a], Weiping Chen[e], Melvin L.K. Chua[b,c,d], Y. Eugene Chinn[f], Chu-Xia Deng[a,*], Ruihong Wang[a,g,2,*]

[a] Faculty of Health Sciences, University of Macau, Macau SAR, China
[b] Division of Radiation Oncology, National Cancer Centre Singapore, Singapore
[c] Division of Medical Sciences, National Cancer Centre Singapore, Singapore
[d] Oncology Academic Programme, Duke-NUS Medical School, Singapore
[e] National Institute of Diabetes and Digestive and Kidney Diseases, Bethesda, MD 20892, United States
[f] Institute of Biology and Medical Sciences, Soochow University School of Medicine, 199# Ren'ai Road, Suzhou Jiangsu 215123, China
[g] Center for Cancer Research, Nation Cancer Institute, National Institutes of Health, Bethesda, MD 20892, United States

ARTICLE INFO

ABSTRACT

Background: Metabolic modulation is capable of maintaining cell potency, regulating niche homeostasis, or determining cell fate. However, little is known regarding the metabolic landscape during early adipogenesis or whether metabolic modulation could be a potential approach for obesity treatment.
Methods: The metabolic footprint during adipocyte commitment was evaluated by metabolomics analysis in mouse embryonic fibroblasts (MEFs). The role of apoptosis induced by ceramide and how ceramide is regulated were evaluated by omics analysis *in vitro*, human database and the adipocyte-specific Sirt1 knockout mouse.
Findings: The metabolic footprint showed that a complicated diversity of metabolism was enriched as early as 3 h and tended to fluctuate throughout differentiation. Subsequently, the scale of these perturbed metabolic patterns was reduced to reach a balanced state. Of high relevance is the presence of apoptosis induced by ceramide accumulation, which is associated with metabolic dynamics. Interestingly, apoptotic cells were not merely a byproduct of adipogenesis but rather promoted the release of lipid components to facilitate adipogenesis. Mechanistically, ceramide accumulation stemming from hydrolysis and the *de novo* pathway during early adipogenesis is regulated by Sirt1 upon epigenetic alterations of constitutive Histone H3K4 methylation and H3K9 acetylation.
Interpretation: The metabolic footprint during adipocyte commitment highlights that apoptosis induced by ceramide is essential for adipogenesis, which is reversed by suppression of Sirt1. Therefore, Sirt1 may constitute a target to treat obesity or other ceramide-associated metabolic syndromes.
Funding: This project was supported by grants from the University of Macau (SRG2015-00008-FHS, MYRG2016-00054-FHS and MYRG2017-00096-FHS to RHW; CPG2019-00019-FHS to CXD) and from the National Natural Science Foundation of China (81672603 and 81401978) to QC.

1. Introduction

In recent years, the incidence rate of obesity and fatty liver has continued to increase globally. In the Behavioral Risk Factor Surveillance System (BRFSS) survey in 2018, at least 30% of adults in the USA were overweight [1]. Mounting evidence suggests that cellular energy metabolic disorders of obesity lead to the development of multiple types of syndromes, such as cardiovascular disease, hypertension, diabetes and inflammation [2−4], and even increase the risk of cancer [5,6]. The expansion of excess adipose tissue can be driven either by adipocyte hypertrophy (the increase of existing adipocyte size) or adipocyte hyperplasia (increase in the number of new adipocytes from precursor differentiation in the process of adipogenesis) [7]. Studies have shown that almost 10% of adult adipocytes continuously turnover each year [8]. However, there is no Food and Drug Administration (FDA) approved drug specifically targeting adipocyte hyperplasia for anti-obesity [9]. We therefore undertook an approach to define the potential target of early adipogenesis for obesity therapy.

* Corresponding authors.
E-mail addresses: cxdeng@um.edu.mo (C.-X. Deng), ruihong.wang@nih.gov (R. Wang).
[1] Co-first author
[2] Lead contact

Research in context

Evidence before this study

Metabolic features are characterized as the comprehensive phenotypes of intrinsic gene transcription, protein abundance, and extrinsic environmental influence, which simultaneously represent a global overview of cellular states. Metabolic modulation of stem cells can maintain stem cell potency or determine cell fate into certain cell types. In contrast to the activated lipid metabolism of differentiated adipocytes or mature adipocytes, little is known regarding the ongoing metabolic footprint during precursors switching into adipogenesis and whether some mechanisms can be fundamental for early adipogenesis, serving as an "Achilles heel" for obesity.

Added value of this study

We depict an ongoing metabolic footprint during adipocyte commitment. Our results uncover a complex array of metabolism enriched as early as 3 h. These metabolic networks tend to fluctuate throughout differentiation. The evolutional metabolic dynamics indicate that apoptosis induced by ceramide is essential for adipogenesis. By 48 h differentiation, the metabolic networks remained focused on ceramide production. Mechanistically, ceramide accumulation stemming from hydrolysis and the de novo pathway during early adipogenesis is effectively regulated by Sirt1 via epigenetic alterations, such as Histone H3K4 methylation and H3K9 acetylation.

Implications of the available evidence

Our studies uncover a tight correlation between metabolic dynamics apoptosis and adipogenesis, which indicates a possible reversible effect by targeting adipocyte apoptosis for obesity treatment. Meanwhile, growing evidence shows that ceramide or ceramide metabolism is associated with a risk of metabolic syndrome, including cardiovascular disease or Alzheimer's disease. Several studies have focused on ceramidases. However, ceramide production is a complicated metabolic process, including the de novo pathway in the ER, hydrolysis of sphingomyelin, and salvage pathway in the lysosome. Thus, targeting single or several gene(s) of ceramide metabolism might lead to an unsuccessful result. Our results demonstrate that modulating ceramide metabolism by Sirt1 might significantly influence current therapeutic strategies for battling obesity and ageing because Sirt1 can effectively decrease different carbon chains of ceramides. This may provide a potential target for obesity treatment or metabolic syndrome by ceramides.

Metabolic features were characterized as the comprehensively causal phenotypes of intrinsic gene transcription, protein abundance, and extrinsic environmental influence, which simultaneously represents a global overview of cellular states [10]. Metabolic modulation of stem cells can maintain stem cell potency or determine cell fate into certain cell types [11−13]. In contrast to the activated lipid metabolism of differentiating adipocytes or mature adipocytes [14], little is known regarding the ongoing metabolic footprint during precursors switching into adipocytes and whether mechanisms can be fundamental for early adipogenesis, serving as an "Achilles heel" for obesity.

Here, the dynamic metabolic footprint during early adipogenesis of mouse embryonic fibroblasts (MEFs) is depicted. A complicated and diversified metabolic network was enriched as early as 3 h and tended to fluctuate throughout differentiation. Subsequently, the spectrum of these perturbed metabolic patterns was limited to some defined metabolic pathways, such as glycerophospholipid

metabolism, pyrimidine metabolism, sphingolipid metabolism, taurine and hypotaurine metabolism, and purine metabolism. These metabolic alterations reached a relatively equipoised state at 48 h of differentiation. Interestingly, all metabolism detected during this period was associated with apoptosis; however, nothing is known about how apoptosis may impact adipogenesis progression.

Apoptosis has been attributed to ceramide accumulation [15−17]. Thus, we initially hypothesized that apoptosis induced by ceramide is indispensable for adipogenesis. Our results suggest that ceramides accumulate and induce apoptosis during early adipogenesis. Inhibition of either ceramide or apoptosis impairs MEF adipogenesis. Interestingly, apoptotic cells are not merely a byproduct of adipogenesis; rather, their release of lipid components is a cue to facilitate adipogenesis. Mechanistically, the increased ceramides stemming from hydrolysis and the de novo pathway are regulated by epigenetic modifications that can be deeply affected by Sirt1.

2. Materials and methods

2.1. Cell line, isolation of primary cells, growth conditions, and plasmids

The 3T3-L1 (ATCC, RRID: CVCL_0123) preadipocyte cell was acquired from ATCC and cultured in DMEM supplemented with 10% bovine serum (Gibco). Primary MEFs were isolated form E12.5 *Sirt1* WT and *Sirt1* KO embryos. Primary white preadipocytes were isolated from inguinal white adipose tissue from 4 week old Sirt1$^{co/co}$ mice following a previous protocol [18].

Lentivirus infection was performed as described. Adenoviruses expressing Cre recombinase and GFP (Ad-Cre) or GFP alone (Ad-GFP) were purchased from the Vector Development Laboratory, Baylor College of Medicine. Adenovirus infection of primary MEFs and white preadipocytes that had a limited lifespan culturing with 20% FBS at 100 MOI as described previously [18].

2.2. Animals

All experiments were approved by University of Macau's Animal Care Ethics Committee and adhere to the guidelines of the Macau's Council on Animal care. Littermate control used for all experiments.

2.3. Adipogenic differentiation

The MEFs, preadipocyte cells and 3T3-L1 cells will be conducted as the model. The differentiation protocol was followed the previous study [19]. Briefly the cells were seeded in a 35 mm dish at a density of 6×10^5 cells/dish. The next day the medium was replaced with DMEM (Thermo Fisher Scientific, 11965118) containing 10% or 20% fetal bovine serum (Thermo Fisher Scientific, 12483020), 0.5 mM IBMX (Sigma-Aldrich, I5807), 0.25 μM dexamethasone (Sigma-Aldrich, D4902), and 1 μg/ml insulin (Sigma-Aldrich, I1505),. After 48 h, change the medium with DMEM with 10% or 20% fetal bovine serum and 1 μg/ml insulin for the first time. The medium is refreshed with the same medium every other 2 days.

2.4. Oil Red O staining

Every other 2 days collect the cells to determinate the state of adipogenesis. Oil Red O staining was performed as described previously [19]. First wash the cell with PBS, then fix the cells with 4% paraformaldehyde (Sigma-Aldrich, 158127) for 30 min. Stain the fixed cells with Oil Red O (Sigma-Aldrich, O0625).

2.5. Determination of FFA, leptin, triglyceride, adiponectin

Obesity related factors including FFA (Njjcbio, A042-2), leptin (Njjcbio, H174) and adiponectin (Njjcbio, H179) were measured according to manufacturer's instruction.

2.6. Metabolomics analysis

The sample preparation for a global metabolic profiling analysis was performed as described previously [20]. Extracted the cell with 60% methanol, and samples were analyzed by UPLC-ESI-QTOF MS using a Waters Acquity BEH C18 (2.1 × 100 mm) 1.7 μm column under the following condition: A, H_2O (0.1% formic acid); B, Acetonitrile; Gradient: initial 98% A to 95% A at 1 min, to 75% A at 2 min, to 45% A at 8 min, to 30% A at 10 min, to 10% A at 13 min, to 5% A at 14 min, to 2% A at 15 min, to 0% A at 17 min before returning to initial conditions at 18.5 min with equilibration for 2 additional minutes. The flow rate was 0.4 mL/minute. The column temperature was maintained at 50 °C. For MS, the conditions were applied as follows: Acquisition mode: MS^E; Ionization mode: ESI positive; Capillary voltage: 2.5 kV (for both positive and negative); Cone Voltage: 30 V; Desolvation temp.: 550 °C; Desolvation gas: 900 L/Hr; Source temp.:150 °C;

Chromatographic data were analyzed using MarkerLynx software (Waters). A multivariate data matrix contains sample information of identity, ion identity (retention time and m/z), and ion abundance was generated through centroiding, deisotoping, filtering, peak recognition, and integration. The intensity of each ion was calculated by normalizing the single ion counts versus total ion counts in the whole chromatogram. And the data matrix was further submitted to the Metaboanalyst (http://www.metaboanalyst.ca/) to analyze.

The sample preparation for ceramide quantification was performed as described previously. Homogenized the cell with 700 μL methanol-H_2O (4:3) and extracted with 800 μL $CHCl_3$ and incubated at 37 °C for 20 min. Centrifuged samples at 13000 g for 20 min, collected the lower phase and evaporated to dryness under vacuum. Suspended the dried sample with 100 μL $CHCl_3$−MeOH (1:1) and using 400 μL Isopropanol-Acetonitrile-H_2O (2:1:1) to dilute the samples. The sample were performed by multiple reaction monitoring (MRM) and/or parent ion scanning using a Waters UPLC-TQD MS.

Waters Acquity BEH C18 (2.1 × 100 mm) 1.7 μm column was used under the following condition: A, H_2O; B, Acetonitrile-Isopropanol (5:2); both A and B contained 10 mM ammonium acetate and 0.1% formic acid. Gradient: initial 70% A to 50% A at 3 min, to 1% A at 8 min and keep it for 7minutes, returned to initial conditions at 16 min with equilibration for 2 additional minutes. The flow rate was 0.4 mL/minute. The column temperature was maintained at 50 °C. For MS, the conditions were applied as follows: Acquisition mode: MS^E; Ionization mode: ESI positive; Capillary voltage: 2.5 kV (for both positive and negative); Cone Voltage: 30 V; Desolvation temp.: 550 °C; Desolvation gas: 900 L/Hr; Source temp.: 150 °C.

2.7. Hydrophilic phase and lipophilic phase separation from apoptotic cells or medium

The Annexin V labelled apoptotic cells were isolated and homogenized with 700 μL methanol-H_2O (4:3), and extracted with 800 μL $CHCl_3$ and incubated at 37 °C for 20 min. Centrifuged samples at 13000 g for 20 min, collected both the lower phase (lipophilic phase) and upper phase (hydrophilic phase), then evaporated to dryness under vacuum. For 48h-differentiation medium, added 400 μL methanol per 300 μL medium. After mixed well, extracted with 800 μL $CHCl_3$ and incubated at 37 °C for 20 min. Centrifuged samples at 13000 g for 20 min, collected both the lower phase (lipophilic phase) and upper phase (hydrophilic phase), then evaporated to dryness under vacuum.

2.8. Quantitative RT-PCR

Total RNA was extracted with Trizol reagent (Theomo Fisher Scientific) according to the manufacturer's instruction. Reverse transcription was performed with the QuantiTect reverse kit (QIAGEN) and Real-time PCR reaction was carried on using SYRB Green Master Mix. Relative quantification was calculated by normalization to its amount of 18S.

2.9. Western blot

The protocol will follow the previous study [21]. The Western Blot was carried out by LI-COR Biosciences with Caspase 3 (CST, #9662; RRID: AB_331439), Caspase 7 (CST, #9492; RRID: AB_2228313), Caspase 8 (CST; #4790), Caspase 9 (CST, #9504; RRID: AB_2275591) antibodies from Cell Signaling. Quantifications of the western blot were performed using ImageJ.

2.10. Transfection and luciferase assay

The transfections were performed with Lipofectamine 2000 (Thermo Fisher Scientific) according to the manufacturer's instructions. Cells were harvested 24 h post-transfection, and luciferase activity was determinated by the dual luciferase reporter assay system (Promega).

2.11. Immunofluorescence and IHC staining

For immunofluorescence, 4% Paraformaldehyde-fixed cells were strained with antibody against ceramide (MAB_0010) from Glycobiotech following the previous protocol [22]. For IHC, sections were deparaffinized, rehydrated, treated for antigen retrieval and stained with Cleaved Caspase 3 antibody (CST, #9661) following the previous protocol [23]. Images were acquired using an LSM710 confocal microscope (Zeiss) and BX53 microscope (Olympus).

2.12. ChIP-Seq and ChIP-qPCR

The ChIP assay was carried out as described previously (Wang et al., 2004). Chromatin was sonicated to shear DNA to a size range of 100−500 bp, and immunoprecipitation was performed with Antibody of H3K4me2 (CST, #9725) and H3K9ac (CST, #9649) purchasing from Cell signaling. Immune complex was collected by Protein A/G Mix Magnetic Beads (Millipore, LSKMAGAG10). Then samples were sent to Novogene to prepare libraries and sequence.

2.13. Data avaliability

The ChIP-Seq data Sequencing data presented in this publication have been deposited in BioProject portal and are accessible [Accession: PRJNA591721; ID: 591721] (https://www.ncbi.nlm.nih.gov/bioproject/?term=PRJNA591721)

2.14. Statistical analysis

Data shown represent the mean ± SEM. At least three biological replicates were performed for all studies using cell cultures. All data were analyzed with t-test, and $p < 0.05$ was considered statistically significant.

3. Results

3.1. Ongoing metabolic footprint during early adipogenesis

Metabolism plays a vital role in dictating whether cells remain quiescent, undergo proliferation or undergo differentiation [10,24,25].

However, little is known regarding the impact of metabolic dynamics on precursors switching into adipocytes. To gain a clear depiction of the ongoing metabolic footprint during early adipogenesis, we began with mouse embryonic fibroblasts (MEFs) as a model system to mimic *in vivo* adipogenesis [26]. Briefly, after treatment with insulin, IBMX, and dexamethasone for 2 days, MEF cultures were maintained with insulin-containing medium for 8 days. Under this condition, wild-type (WT) MEF cells differentiated into adipocytes and synthesized more oil droplets along with adipogenesis progression (Supplementary Fig. 1a and b). Klf5 and C/EBPβ, which are induced at the early stage of adipocyte differentiation, increased until they peaked at 2 d [27,28], indicating that the early adipogenesis of MEFs occurs within a time scale of 2 d (Supplementary Fig. 1c and d; $p < 0.05$ for 2 d and 4 d). Thus, we performed a global metabolomics analysis to trace metabolic dynamics of MEFs within 48 h of adipogenesis. Based on the features of metabolite species or contents, the early adipogenesis progression of MEFs was clustered into 3 distinct sets, in which a considerable difference in metabolic features was revealed between normal and the 48 h-differentiated cell populations. Notably, the dramatic similarity of metabolic patterns was observed in the 3−24 h differentiated MEFs. These characteristics fluctuated between 0 h and 48 h-differentiated cells, suggesting that the temporal interval of 3−24 h was the tipping point of adipocyte commitment (Fig. 1a and b). After identifying potential metabolites with significant fold change, metabolism analysis was performed (Fig. 1c). Under normal conditions, the WT MEFs displayed metabolic features, including selenoamino acid, pyruvate and arachidonic acid metabolism. In the tipping points from 3 h to 24 h, a greater diversity of metabolism was activated, which tended to fluctuate throughout differentiation. Subsequently, at 48 h of differentiation, the metabolic changes slowed to a limited spectrum, including glycerophospholipid metabolism, pyrimidine metabolism, sphingolipid metabolism, taurine and hypotaurine metabolism, and purine metabolism. Interestingly, the committed cells after 48 h of induction presented characteristics of "qualified" adipocytes, as evidenced by activated lipid fatty acid elongation in mitochondria and fatty acid metabolism (Fig. 1d), which further suggests that MEF fate is determined in adipocytes within 48 h. From these results, we conclude that the ongoing metabolic dynamics of early adipogenesis progression are not monotonic and gradual but pass through nonlinear and drastic transitions to reach a relatively balanced state after 48 h of differentiation, which include glycerophospholipid metabolism, pyrimidine metabolism, sphingolipid metabolism, taurine and hypotaurine metabolism, and purine metabolism.

3.2. Co-occurrence of apoptosis and adipogenesis *in vitro and* in vivo

In WT MEFs, several common metabolic pathways, such as taurine and hypotaurine metabolism, glycerophospholipid metabolism, sphingolipid metabolism, pyrimidine metabolism, and purine metabolism, were enriched in the first 48 h (Fig. 1e). Interestingly, these common pathways are all related to apoptosis. To verify the metabolomics analysis results, apoptosis was measured *in vitro* and *in vivo*. Increased cell blebbing (Fig. 2a) and elevated TUNEL-positive populations were observed (Fig. 2b) during early adipogenesis. Meanwhile, Caspase 3 activation was also observed *in vivo* during the development of adipose tissues (Fig. 2c). These evidence suggest that some metabolites might function as a link between adipogenesis and apoptosis.

3.3. Apoptosis is essential for early adipogenesis

Apoptosis is an essential biological process during development. It serves to remove superfluous parts or signal to promote communication from parts to the whole, especially in nervous system development, muscle patterning, and cardiac morphogenesis [29]. However, little is known regarding the functional significance of apoptosis

during adipogenesis. To gain insight into the role of apoptosis in adipogenesis, we first blocked apoptosis of MEFs by Z-VAD-Fmk treatment during adipogenesis progression. The results showed that Z-VAD-fmk could decrease lipid droplet formation (Fig. 2d) and significantly reduce the expression of adipogenesis-associated principal regulators, including PPARγ (Fig. 2e) and C/EBPα (Fig. 2f). Furthermore, acute RNAi-mediated knockdown of caspase 3 resulted in less adipogenesis of 3T3-L1 cells as revealed by oil red O analysis (Fig. 2g), which was accompanied by decreased expression of PPARγ (Fig. 2h) and C/EBPα (Fig. 2i). To further confirm the effect of apoptosis on adipogenesis *in vivo*, pre-adipocytes were isolated from WT mice and induced for adipogenesis after infection with lentivirus-shControl or shCaspase 3. This analysis demonstrated that loss of caspase 3 impaired the differentiation capacity of pre-adipocytes (Fig. 2j−l). These observations demonstrate that apoptosis is an essential process for adipocyte differentiation.

3.4. Apoptotic cells provide nutritions to promote adipogenesis

We next investigated the function of apoptosis in the adipogenesis process. When 3T3-L1 cells were treated with Annexin V-positive cells, we observed elevated levels of oil droplets (Fig. 3a; $p < 0.05$ for 2d, 4d and 6d) that was accompanied by significantly increased PPARγ or C/EBPα expression (Fig. 3b and c; $p < 0.05$ for 2d, 4d and 6d of PPARγ expression; $p < 0.05$ for 2d and 4d of C/EBPα expression). Mechanistically, apoptotic cells could elevate both PPARγ and C/EBPα promoter activities (Fig. 3d and e). These data suggest that apoptotic cells might provide factors to facilitate adipogenesis.

To further understand the role of apoptotic populations in adipogenesis, the hydrophilic and lipophilic phases of apoptotic cells were utilized to treat 3T3-L1 cells during adipogenesis progression. Compared with the hydrophilic phase-treated group, the lipophilic phase of apoptotic cells dramatically promoted adipogenesis (Fig. 3f−h). All of the above data indicate that apoptotic cells might breakdown to release lipid groups, which accommodate the cells to commit to adipocyte differentiation.

Fatty acids enhance lipid droplet synthesis by modulating the expression of enzymes of fatty acid metabolism [30,31]. Thus, we next examined whether apoptotic cells could provide fat components to facilitate adipogenesis. The medium from 48 h-differentiated cells was collected and named "apoptotic medium". Apoptotic medium elevated the promoter activity of PPARγ and C/EBPα to upregulate oil droplet generation (Fig. 3i−k). To better understand the active components, the collected apoptotic medium was separated into hydrophilic and lipophilic phases by methanol-chloroform extraction, and the extracts were utilized to treat 3T3-L1 cells. Compared to normal medium, the lipophilic component of differentiation medium triggered more oil droplet production, but no effect was observed with the hydrophilic components (Fig. 3l). Moreover, the differentiation-inducing medium at 48 h contained more FFA compared to normal differentiation-inducing medium (Supplementary Fig. 2a). Taken together, these results support the idea that apoptotic cells direct adipocyte differentiation by providing lipid components.

3.5. Ceramide triggers apoptosis and facilitates adipogenesis

We further investigated the initiation process and function of apoptosis during adipogenesis. Since ceramide is a stand-out target from our global metabolomic analysis, and itself is a very well documented factor that drives the apoptosis process [15−17], we decided to examine the ceramide content in apoptotic cells during adipogenesis. In the previous global metabolomic analysis, we followed a standard extraction method of 60% methanol based on metabolomics profiles. Because ceramides are a class of lipid with limited water-solubility, we switched to a lipid extraction method to maximally enrich ceramides. 3T3-L1 cells were induced into adipogenesis for 24 h and then
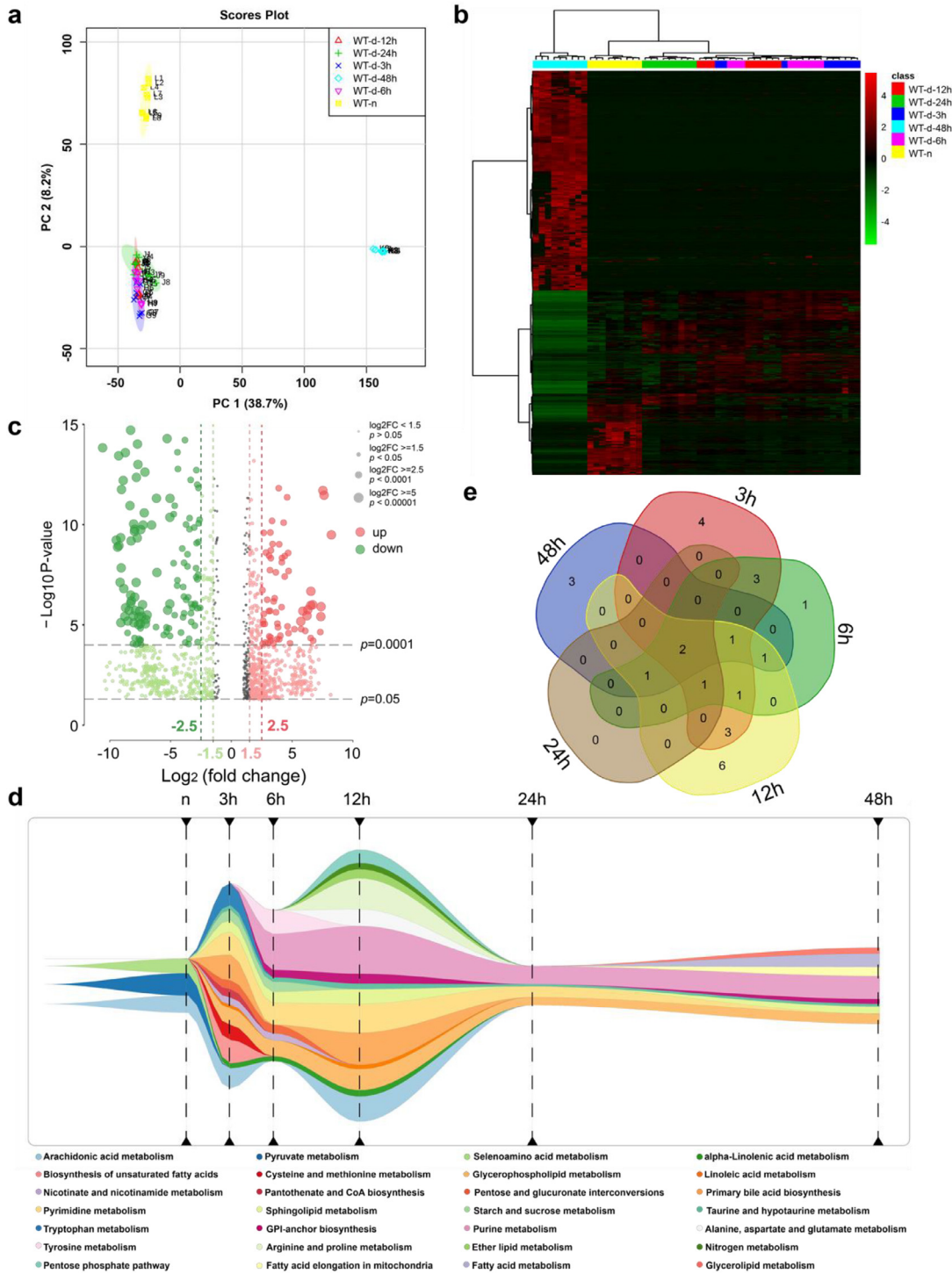
Fig. 1. Ongoing metabolic footprint during the early adipogenesis. (a) PLS-DA analysis of WT KO MEFs metabolites during early stage adipogenesis. (n = 9 for each group). (b) The heatmap of WT MEFs metabolites during early stage adipogenesis. (c) Volcano Plot of metabolites from 0 h and 3 h group of WT MEFs, which was used to set the range of target metabolites to be identified. (n = 9 for each group) (d) The metabolic landscape of WT MEFs at the early adipogenesis progression. The metabolisms were activated and tend to fluctuate throughout differentiation time, which includes selenoamino acid metabolism, pyruvate metabolism and arachidonic acid metabolism in normal condition; glycerophospholipid metabolism, linoleic acid metabolism, arachidonic acid metabolism, taurine and hypotaurine metabolism, alpha-Linolenic acid metabolism, nicotinate and nicotinamide metabolism, pantothenate and CoA biosynthesis, pentose and glucuronate interconversions, starch and sucrose metabolism, sphingolipid metabolism, cysteine and methionine metabolism, tryptophan metabolism, pyrimidine metabolism, biosynthesis of unsaturated fatty acids, primary bile acid biosynthesis in 3h-differentiation; sphingolipid metabolism, glycerophospholipid metabolism, taurine and hypotaurine metabolism, alpha-Linolenic acid metabolism, nicotinate and nicotinamide metabolism, GPI-anchor biosynthesis, pentose and glucuronate interconversions, starch and sucrose metabolism, pyrimidine metabolism, tyrosine metabolism and purine metabolism in 6h-differentiation; glycerophospholipid metabolism, pyrimidine metabolism, taurine and hypotaurine metabolism, alpha-Linolenic acid metabolism, sphingolipid metabolism, alanine, aspartate and glutamate metabolism, Linolenic acid metabolism, nitrogen metabolism, ether lipid metabolism, GPI-anchor biosynthesis, pentose phosphate pathway, purine metabolism, arachidonic acid metabolism, arginine and proline metabolism, primary bile acid biosynthesis and steroid hormone biosynthesis in 12h-differentiation; taurine and hypotaurine metabolism, glycerophospholipid metabolism, pyrimidine metabolism and purine metabolism in 24h-differentiation; taurine and hypotaurine metabolism, glycerophospholipid metabolism, GPI-anchor biosynthesis, sphingolipid metabolism, purine metabolism, fatty acid elongation in mitochondrial and fatty acid metabolism in 48h-differentiation. (e) The Venn diagram of the identified metabolisms of MEFs during the early adipogenesis, in which glycerophospholipid metabolism, pyrimidine metabolism, sphingolipid metabolism, taurine and hypotaurine metabolism, and purine metabolism were frequently enrichment. Results are expressed as mean±SEM. *Student's t-test* was used for the statistical analysis; **p < 0.01, *p < 0.05.
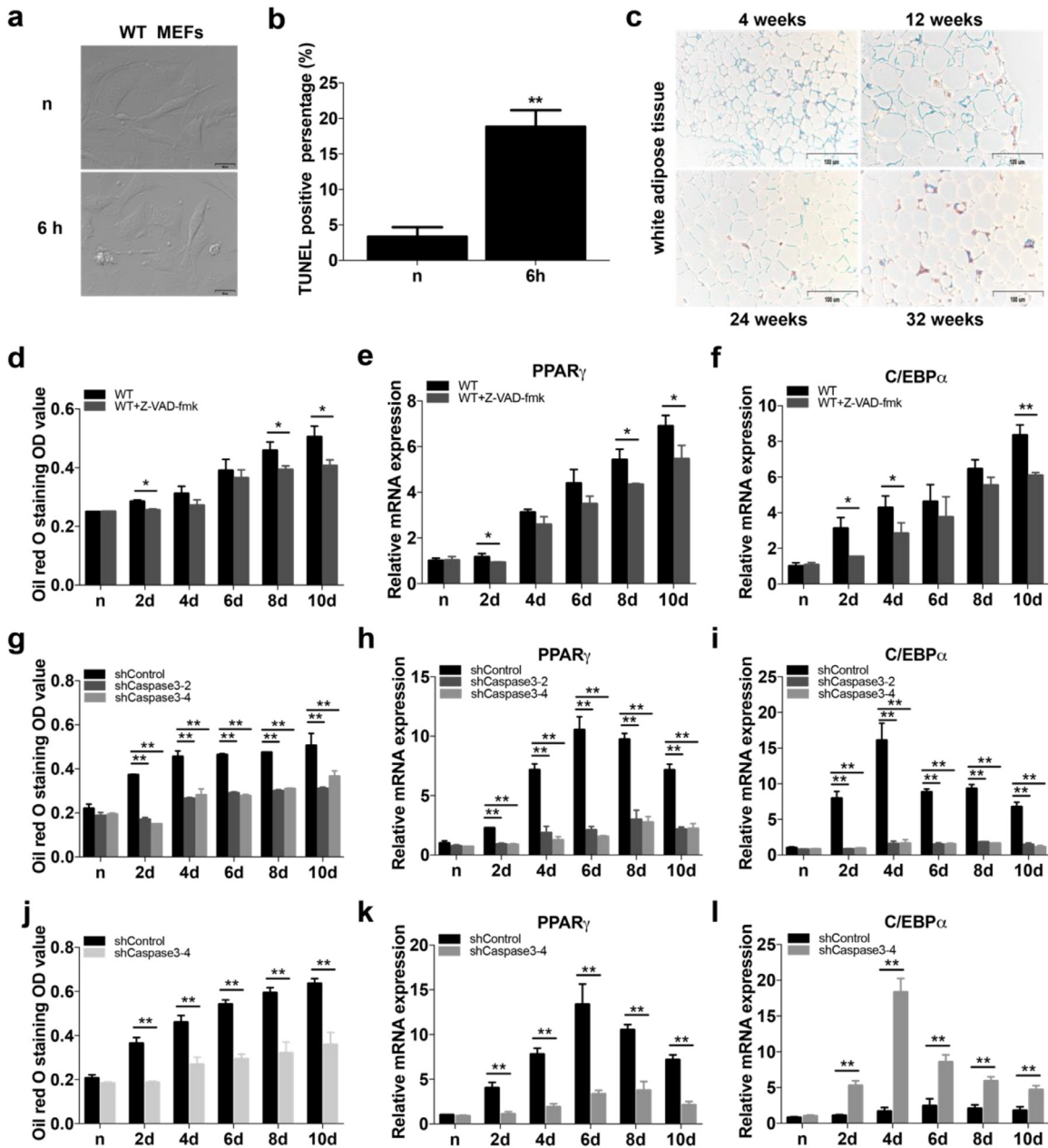
Fig. 2. Apoptosis is essential for the early adipogenesis. (a-b) Apoptosis occurred in the early stage of adipogenesis of MEFs (a) and apoptotic population percentage (b) of WT MEFs in 24h-differentiation (n = 3 for each group). Scale bar 100μm.(c) IHC staining of cleaved Caspase 3 in the inguinal fat tissues from WT mice from 4-week to 32- week old (n = 6 for each group). Scale bar 100μm. (d) Quantification of Oil Red O staining result of WT MEFs after Z-VAD-frm treatment during adipogenesis (n = 3 for each group). (e and f) The mRNA level PPARγ (e), C/EBPα (f) of WT MEFs after Z-VAD-frm treatment during adipogenesis (n = 3 for each group). (g) Quantification of Oil Red O staining result of 3T3-L1 infected with lentivirus-shCaspase3 during adipogenesis (n = 3 for each group). Two independent sh-caspase 3 constructs were used. (h and i) The mRNA level PPARγ (h), C/EBPα (i) of 3T3-L1 infected with lentivirus-shCaspase3 during adipogenesis (n = 3 for each group). (j) Quantification of Oil Red O staining result of isolated preadipocyte infected with lentivirus-shCaspase3 during adipogenesis (n = 3 for each group). (k and l) The mRNA level PPARγ (k), C/EBPα (l) of isolated preadipocyte infected with lentivirus-shCaspase3 during adipogenesis (n = 3 for each group). Results are expressed as mean±SEM. *Student's t-test* was used for the statistical analysis; **p < 0.01, *p < 0.05.

labelled with Annexin V-Alexa 594. The apoptotic cells were sorted from the non-apoptotic cells. Compared to the isolated non-apoptotic cells, there was a dramatic upregulation in the level of total ceramides in the apoptotic cell population (Fig. 4a). Moreover, immunofluorescence analysis of the 3T3-L1 cells differentiated for 24 h revealed that ceramides accumulated in apoptotic cells (Fig. 4b). We also asked whether ceramide itself could induce apoptosis in our system. We observed caspase 3 activation in WT MEFs following ceramide treatment (Fig. 4c). Consistent with this finding, treatment with ceramide-specific inhibitors, GW4869 and PIK93 [32,33], blocked apoptosis and delayed/reduced adipogenesis efficiency (Fig. 4d and e). These findings suggest that ceramide triggers apoptosis in the early stages of adipogenesis. Several acute RNAi-mediated knockdowns of ceramide-related genes from hydrolysis and *de novo* pathways, such as *Cers1, Cers2, Cers3,* and *Smpd1*, resulted in decreased ceramide levels during 24 h of differentiation (Supplementary Fig. 3a-c). Furthermore, oil droplet accumulation was reduced in the presence of *Cers1, Cers2, Cers3,* and *Smpd1* knockdown (Supplementary Fig. 3d-i). Of note, the ceramide content tended to decline after caspase 3 inhibitor treatment (Fig. 4f). The above evidence argues that, during adipogenesis, ceramide promotes cells to undergo apoptosis; in a positive feedback loop, apoptotic cells then release more ceramide. Thus, ceramide is an essential metabolite for adipogenesis. Apoptosis is therefore a critical process underpinning adipogenesis for two reasons: 1) as
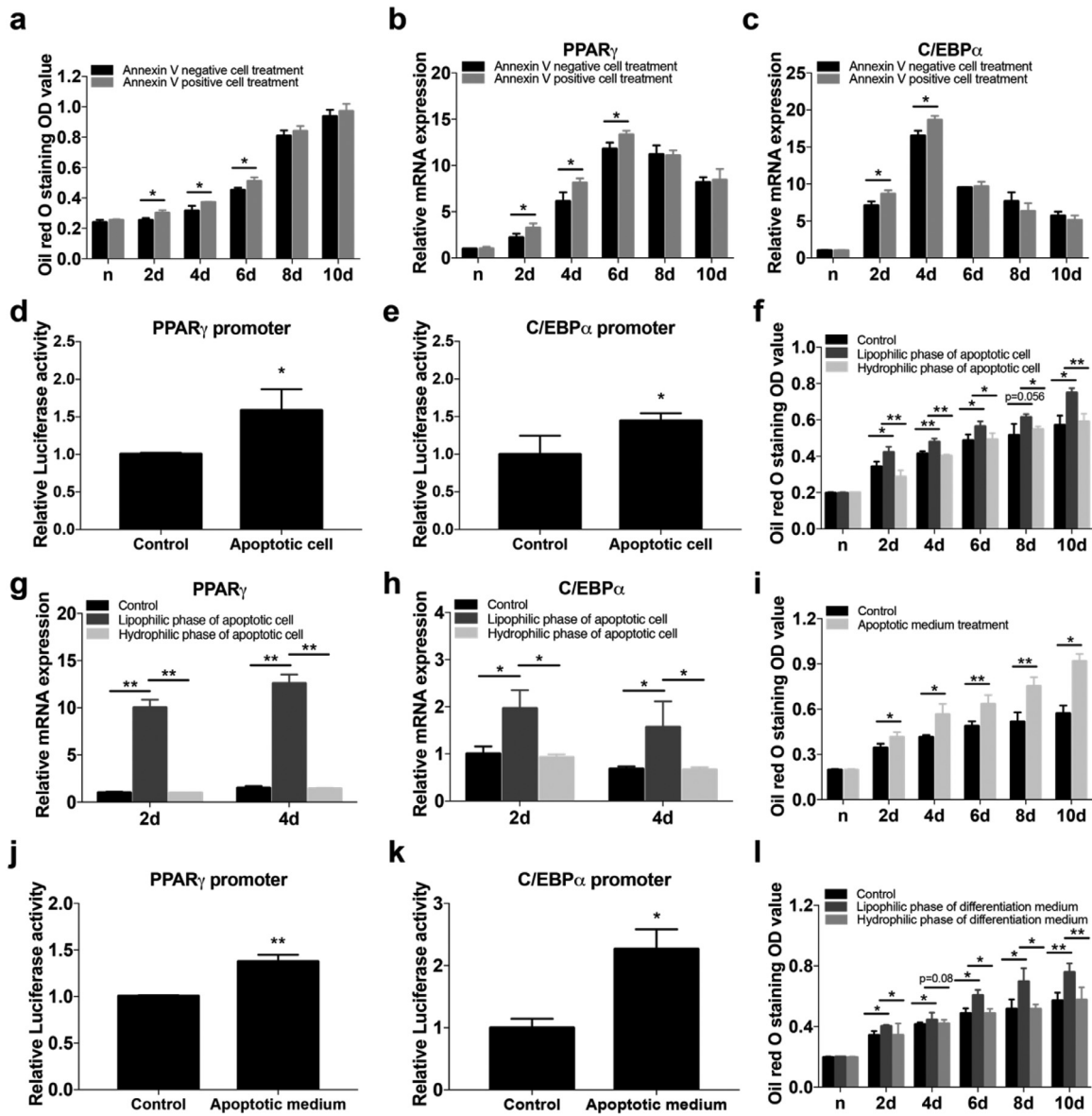
Fig. 3. Apoptotic cells provide nutritions to promote adipogenesis. (a) Quantification of Oil Red O staining result in 3T3-L1 cells that were co-cultured with Annexin V positive cells (apoptotic cells) which number was equal to 40% differentiating cell density during adipogenesis (n = 3 for each group). (b and c) The mRNA level PPARγ (b), C/EBPα (c) of 3T3-L1 that were co-cultured with Annexin V positive cells (apoptotic cells) which number was equal to 40% differentiating cell density during adipogenesis (n = 3 for each group). (d-e) Luciferase activity of PPARγ promoter (d) and C/EBPα promoter (e) in 3T3-L1 cells treated by apoptotic cells, apoptotic cells plus ceramide for 48 h differentiation (n = 3 for each group). (f) Quantification of Oil Red O staining result of 3T3-L1 cell treated by lipophilic and hydrophilic phase extracted from apoptotic cells. (n = 3 for each group). (g-h) The mRNA level PPARγ (g), C/EBPα (h) of 3T3-L1 cells treated by concentrated lipophilic phase and hydrophilic phase extracted from apoptotic cells. (n = 3 for each group). (i) Quantification of oil red O staining result of 3T3-L1 cell treated by concentrated medium from 48h-differentiation (n = 3 for each group). (j-k) Luciferase activity of PPARγ promoter (j) and C/EBPα promoter (k) of 3T3-L1 cells treated with concentrated 48h-differentiation medium for 48 h differentiation (n = 3 for each group). (l) Quantification of Oil Red O staining result of 3T3-L1 cell treated by concentrated lipophilic phase and hydrophilic phase extracted from 48h-differentiation medium for adipogenesis (n = 3 for each group). Results are expressed as mean±SEM. *Student's t-test* was used for the statistical analysis; $**p < 0.01$, $*p < 0.05$.

positive feedback for increased ceramide content upstream, and 2) as a provider of ceramide for downstream adipogenesis.

Previous reports have shown that C/EBPα expression is upregulated by ceramide treatment after 24 h of differentiation, which implies a time-dependent effect of ceramide [34]. To identify the "time-window" in which ceramide promotes adipogenesis, C6-ceramide was added into the culture at different times after induction of adipogenesis. Upregulated PPARγ expression was detected upon C6-ceramide treatment after 24 h of differentiation (Fig. 4g). Additionally, treating MEFs with ceramide generated more oil droplets (Fig. 4h). Furthermore, we investigated whether the PPARγ and C/EBPα promoters could be directly affected by ceramide levels. As expected, C6-ceramide treatment elevated PPARγ and C/EBPα

promoter activity (Fig. 4i and j). In support of this, treatment of differentiating cells containing the two promoter constructs with the caspase 3 inhibitor Z-VAD-FMK and Fumonisin B, a ceramide inhibitor, reduced corresponding luciferase activity (Fig. 4i and j). Together, these data demonstrate that ceramide serves as a promoting factor for PPARγ and C/EBPα transcription in adipogenesis.

3.6. Ceramide accumulation at the early stage of adipogenesis is enhanced by epigenetic modifications in the absence of Sirt1

Given that ceramides can be produced from both *de novo* and hydrolysis pathways [35], specific ceramide synthesis inhibitors were used to identify the pathways involved. Treatment with PIK93, which
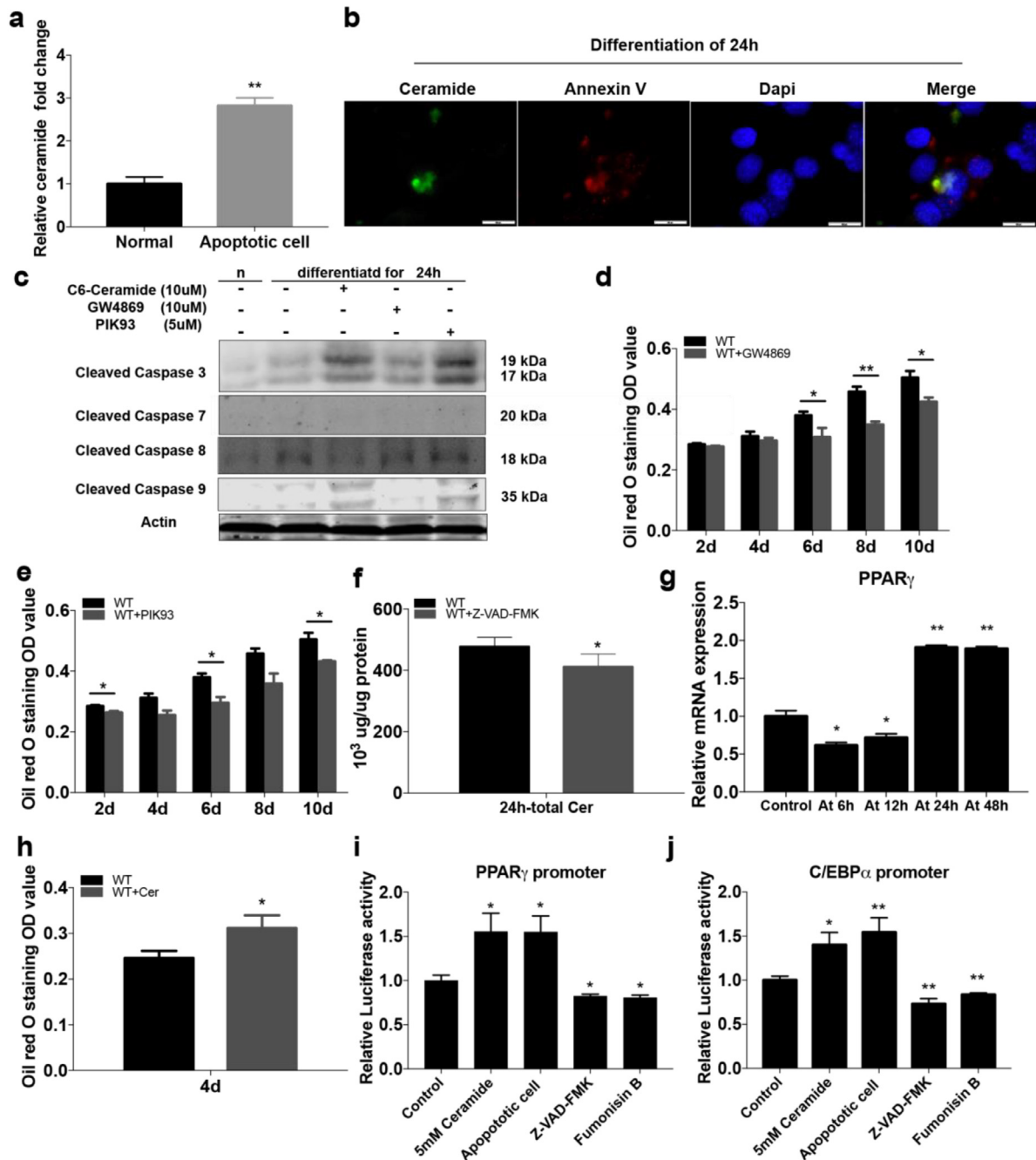
Fig. 4. Ceramide triggers apoptosis and facilitates adipogenesis. (a) Apoptotic cells (Annexin V positive) had more ceramide than the non-apoptotic cells (Annexin V negative). The cells were separated by flow cytometry from 3T3-L1 cells differentiated for 24 h (n = 3 for each group). (b) Co-localization of ceramide with apoptotic cell (Annexin V positive) in 3T3-L1 cells differentiated for 24 h. Scale bar 100μm. (c) Ceramide treatment promoted apoptosis progress. Conversely, ceramide inhibitor GW4869 and PIK93 inhibit apoptosis determined by Western Blot analysis of MEFs differentiated for 24 h (n = 3 for each group). (d and e) Quantification of Oil Red O staining result of WT MEFs by ceramide inhibitor GW4869 (d) and PIK93 (e) treatment after 24 h differentiation during adipogenesis (n = 3 for each group). (f) Ceramide content of WT MEFs by apoptosis inhibitor Z-VAD-frm treatment for 24 h differentiation (n = 6 for each group). (g) The mRNA level PPARγ of 3T3-L1 treated with 5 mM ceramide at different time points (n = 3 for each group). (h) Quantification of Oil Red O staining result of WT MEFs by 5 mM ceramide treatment after 24 h differentiation for adipogenesis (n = 3 for each group). (i-j) Luciferase activity of PPARγ promoter (i) and C/EBPα promoter (j) of 3T3-L1 cells treated by ceramide and apoptotic cells (Annexin V positive cell) respectively at 48 h post differentiation (n = 6 for each group). Results are expressed as mean±SEM. *Student's t-test* was used for the statistical analysis; **$p < 0.01$, *$p < 0.05$.

inhibits ceramide shuttling between the ER and Golgi compartment and thereby inhibits the *de novo* pathway [36], inhibited adipogenesis in WT MEFs (Fig. 4e). Additionally, inhibition of ceramide generation from the hydrolysis pathway by GW4869 and 3-O-Methyl-sphingo-myelin, a natural SMase inhibitor [37,38], blocked the oil droplet accumulation during adipogenesis (Fig. 4d and Supplementary Fig. 4a). However, D-PDMP, a lactosylceramide inhibitor [39], displayed no effect on adipogenesis (Supplementary Fig. 4b). This was further corroborated by qRT-PCR analysis in which most ceramide-related

genes of the *de novo* synthesis and hydrolysis pathways were elevated in WT MEFs that were differentiated for 24 h (Fig. 5a). Considering that diverse gene pools of ceramide metabolism were switched on during this process, we postulated that increased ceramide during early adipogenesis is manipulated by specific epigenetic alterations. Indeed, analysis of these ceramide-related genes by Enricher database indicated that H3K4 methylation and H3K9 acetylation were critical for promoting ceramide production (Supplementary Fig. 4c and Supplementary Table 1).

Sirt1 is a well-known histone deacetylase, and it has also been demonstrated to bind to MLL members to affect histone H3K4 methylation levels [40]. Hence, we hypothesized that this effect could arise from epigenetic dysregulation of their promoters modulated by Sirt1. Consistent with this hypothesis, Western blot analysis with our own samples from the early stage of adipogenesis revealed that levels of H3K4me2 and H3K9ac were increased after 24 h of adipogenesis induction, and Sirt1 KO MEFs displayed higher histone H3K4 dimethylation and histone H3K9 acetylation compared with WT MEFs at this time point (Fig. 5b). Next, we performed ChIP-seq to investigate whether the abovementioned epigenetic modifications were enriched at the transcription start sites of the promoters of these ceramide metabolic genes. As expected, in MEFs differentiated for 24 h, the promoter regions of PPARγ, C/EBPα, PRDM16, and FABP4 were increasingly enriched to peak levels consistent with a previous study (data not shown here) [18]. Likewise, compared with wildtype MEFs, Sirt1 KO MEFs displayed almost twice the amount of genes whose promoter regions were enriched in binding to H3K9ac; surprisingly, Sirt1 KO MEFs showed a 40-fold higher number of promoters that are enhanced with the H3K4me2 marker (Fig. 5c). To visualize the global variation in gene expression patterns by these epigenetic modifications during the early stage of adipogenesis, we plotted the averaged and normalized peak of genes in the targeted pathways. Sirt1 deficiency was associated with more promoters from adipogenesis (Fig. 5d), apoptosis (Fig. 5e), sphingolipid metabolism (Fig. 5f), and ceramide pathways (Fig. 5g), with enriched Pol II, H3K9ac and H3K4Me2 binding. The enhanced binding of promoters was most pronounced around the transcription start site, implying elevated gene expression. Several ceramide-related gene promoters were compared and validated by ChIP-qPCR (Fig. 5h and i, and Supplementary Fig. 4d-f). Absence of Sirt1 resulted in increased ceramide production during MEF adipogenesis (Fig. 5j and Supplementary Fig. 4 g). We also employed a ChIP-qPCR to study the dynamic histone alterations in a kinetic fashion. We observed that the distribution of promoter region enrichment of apoptosis genes (Cxcl5 and Emec6) fluctuated (Supplementary Fig. 4h-k), consistent with the change in ceramide content during adipogenesis (Fig. 5j). When Sirt1 was overexpressed in 3T3-L1 cells, the levels of H3K4me2 and H3K9ac decreased after 24 h of adipogenesis induction (Supplementary Fig. 5a and b). Furthermore, Sirt1 overexpression inhibited ceramide production (Supplementary Fig. 5c-e). These data demonstrate that ceramide production can be effectively modulated by Sirt1 via epigenetic alterations.

3.7. Ceramide-related genes are negatively correlated with Sirt1 expression in human adipose tissues

Given that ceramide production is enhanced in the absence of Sirt1 by epigenetic modifications during MEF adipogenesis, we explored whether this causal relationship is consistent with non-diabetic obese patients by analysing related gene expression alterations in the human database (GSE2508). Here, human abdominal subcutaneous adipose tissues were utilized to retrieve RNA-Seq data. Compared with non-obese subjects, whose average BMI (body mass index) was 25 kg/m^2, the expression of Sirt1 was significantly declined in adipose tissues from obese patients whose BMI was >45 kg/m^2 (Fig. 6a). The obese subjects also displayed a dramatic increase in the expression of genes involved in the apoptosis, sphingolipid and ceramide-related pathways (Fig. 6b), consistent with the ChIP-seq analysis of MEFs (Fig. 5d−g). Furthermore, the genes that participate in ceramide production from the de novo and hydrolysis pathways, including Sptlc2 (Supplementary Fig. 6a) and Smpd1 (Supplementary Fig. 5c), were significantly elevated in the obese group, whereas Kdsr (Supplementary Fig. 6b), Smpd3 (Supplementary Fig. 6d) and B4galt6 (Supplementary Fig. 6e) displayed the same increasing trend in the obese group. Genes of ceramide synthase, including

Cer1, Cers2, and Cers3, did not differ between lean and obese individuals (Supplementary Fig. 6f-h). Since the human adipose samples in the database were obtained from individuals aged >24 years old, who were not at a stage of vigorous adipogenesis [41], the fate-switching cells were inclined to obtain ceramide from the de novo pathway rather than hydrolysis. Further data mining revealed significant negative correlations of Sirt1 with genes in the apoptosis pathway ($R = -0.6$; $p < 0.01$), sphingolipid pathway ($R = -0.68$; $p < 0.01$), and ceramide-related pathway ($R = -0.4$; $p < 0.01$) (Fig. 6c−e). Of note, analysis of adipose stem cells (ASC) of human subcutaneous WAT from the public database displayed that morbidly obese individuals had lower expression of Sirt1 and higher expression of genes involved in regulating the ceramide pathway in comparison to non-obese individuals (Fig. 6f).

3.8. Modulating ceramide levels by Sirt1 provides a potential target for obesity treatment

To directly test whether manipulating ceramide levels by Sirt1 is a potential target for obesity treatment, several parameters were investigated using in vitro and in vivo experiments. Sirt1, acting as an energy sensor depending on the intracellular NAD$^+$/NADH ratio [42,43], might be involved in balancing cellular metabolic states to attenuate the function of ceramide metabolism in adipocyte commitment. To investigate this point, the metabolite pattern between Sirt1 KO and WT MEFs was compared. Under normal conditions, Sirt1 WT MEFs displayed metabolic features that covered selenoamino acid, pyruvate and arachidonic acid metabolism (Supplementary Fig. 7a). In contrast, GPI-anchor biosynthesis and glycerophospholipid metabolism were the major features of normal Sirt1 KO MEFs (Supplementary Fig. 7b). Interestingly, this divergence in metabolic profiles was reduced at the transition from both the Sirt1 WT and Sirt KO MEFs into adipocytes (Fig. 7a and Supplementary Fig. 7c). Similar to Sirt1 WT MEFs, several common metabolic pathways, taurine and hypotaurine metabolism, glycerophospholipid metabolism, sphingolipid metabolism, and GPI-anchor biosynthesis were enhanced in Sirt1 KO MEFs, and all are related to the apoptosis process (Supplementary Fig. 7d). These data indicate that Sirt1 deficiency targets ceramide to push adipogenesis progression rather than alter adipocyte fate or remodel metabolism in response to inducing signals.

Loss of Sirt1 resulted in increased ceramide production (Fig. 5j). Furthermore, most of the genes involved in the de novo synthesis and hydrolysis pathways were more upregulated in Sirt1 KO MEFs compared with WT MEFs, which led to an extensive increase of different chains of ceramide (Fig. 7b and c). Thus, Sirt1 can effectively maintain ceramide homeostasis during early adipogenesis.

Cumulative evidence indicates that Sirt1 can inhibit adipogenesis [44−46]. To further underpin ceramide's function in adipogenesis, the capacity of Sirt1$^{-/-}$ MEFs to differentiate into adipocytes in the absence of ceramide was investigated. Of note, treatment with PIK93 inhibited adipogenesis in Sirt1 KO and WT MEFs (Fig. 7d). Additionally, inhibition of ceramide generation by GW4869 and 3-O-Methylsphingomyelin was sufficient to block MEF adipogenesis in the absence of Sirt1 (Fig. 7e and f). This suggests that ceramide is crucial for the upstream regulation of adipogenesis by Sirt1. Similarly, adipogenic characteristics were observed in ATKO (the adipocyte-specific Sirt1 knockout) mice (Supplementary Fig. 8a and b), including increased body weight (Supplementary Fig. 8c), increased inguinal or epididimal fat (Supplementary Fig. 8d and e), higher serum FFA and leptin levels, and lower adiponectin levels ($p < 0.01$) (Supplementary Fig. 7i-k). In contrast, there was no significant difference in the body length or liver weight among these groups (Supplementary Fig. 8 g, h). Importantly, mass spectrometry revealed that white adipose tissue from Sirt1 ATKO mice contained higher ceramide content compared to the white adipose tissue from WT mice (Fig. 7g). Furthermore, exon array analysis revealed significant apoptotic
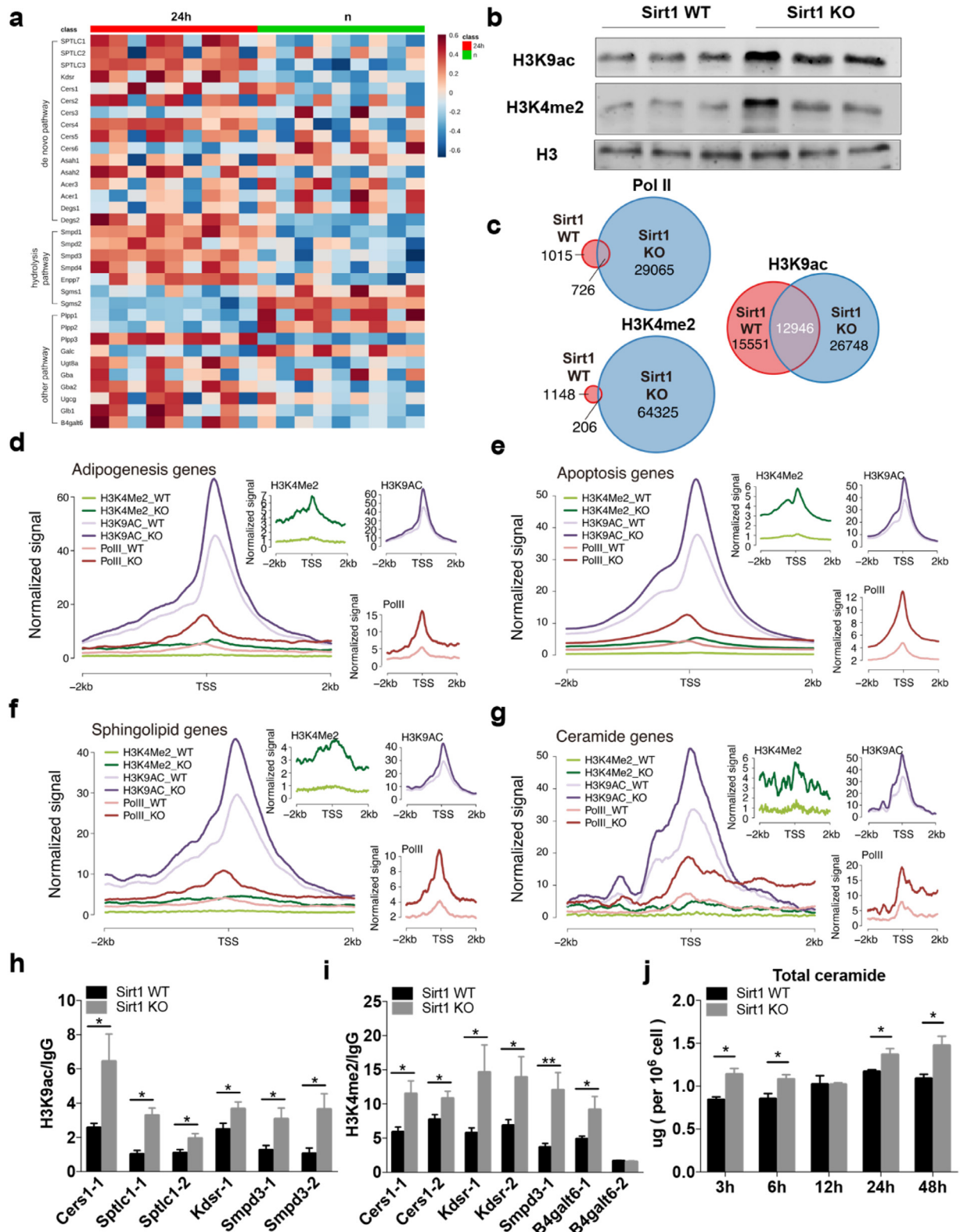
Fig. 5. Ceramide accumulation at early stage of adipogenesis is enhanced by absence of Sirt1 via epigenetic modification. (a) The expression of genes that are involved in ceramide production was analyzed by Q-PCR in WT MEF cells ($n = 9$ for each group). (b) Western blot analysis to show the level of H3K9ac and H3K4me2 in Sirt1 WT and Sirt1 KO MEFs post 24 h differentiation. (c) Vann-Den graphs to show the global status of ChIP-Seq data. More gene promoter sites were enrichment in Sirt1 KO MEF cells than in Sirt1 WT MEF cells for 24 h differentiation. (d-g) Pol II, H3K4me2 and H3K9ac enrichment at the transcription start sites on apoptosis pathway (d), adipogenesis pathway (e), Sphingolipid metabolism (f) and ceramide pathway genes (g) promoters. (h and i) ChIP-qPCR validation of H3K9ac and H3K4me2 enrichment on Cers1, Sptlc1, Kdsr, Smpd3 and B4galt6 promoters in Sirt1 WT and Sirt1 KO MEFs ($n = 3$ for each group). (j) Ceramide content analyzed by UPLC-MS in Sirt1 WT and Sirt1 KO MEF cells during early stage adipogenesis process ($n = 3$ for each group). Results are expressed as mean±SEM. Student's t-test was used for the statistical analysis; **$p < 0.01$, *$p < 0.05$.
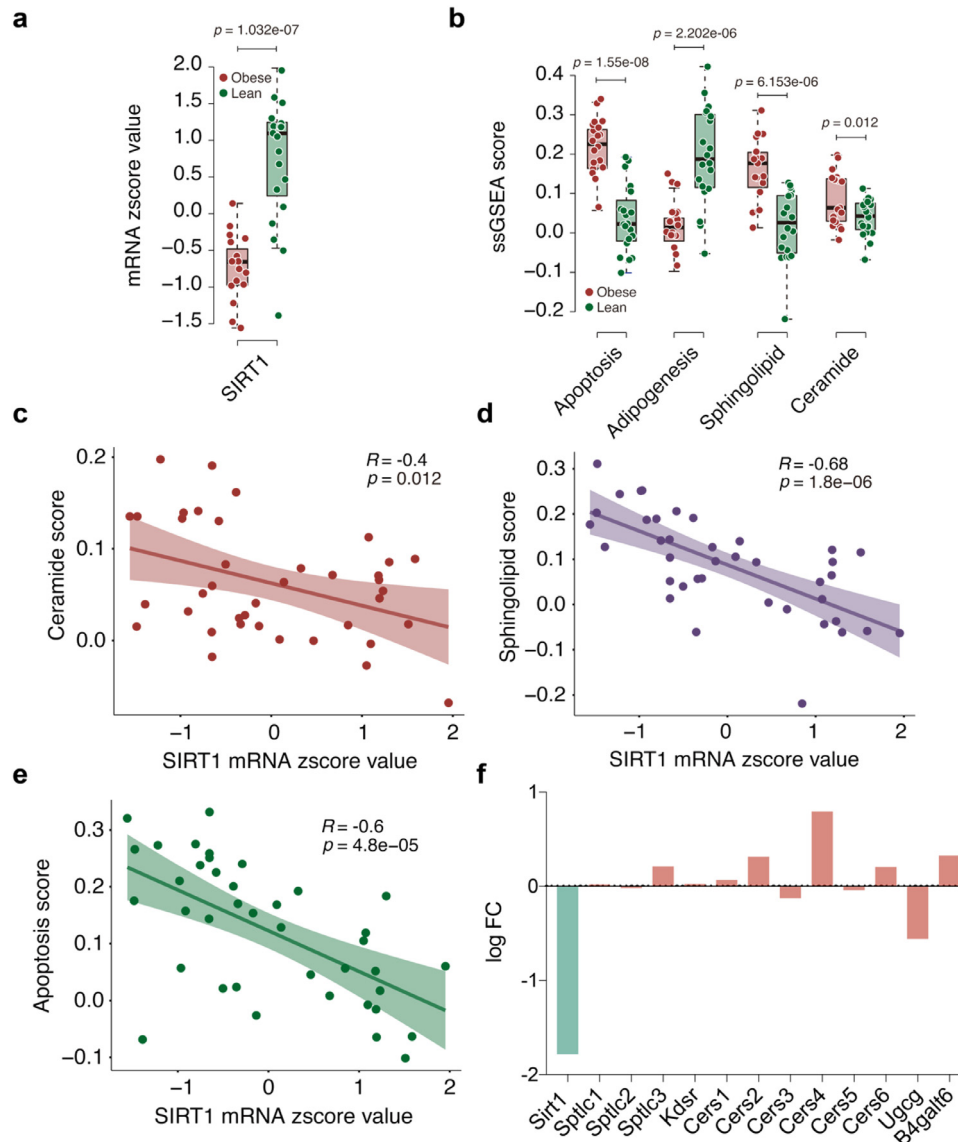
Fig. 6. Ceramide-related genes negatively correlate with Sirt1 expression in human adipose tissues. (a) The expression of Sirt1 was significantly decreased in adipose tissue of obese patients whose BMI is > 45 kg/m^2 (GSE2508). (b) The obese subjects also showed a dramatically increase in the apoptosis pathway, sphingolipid pathway and ceramide related pathway, but a decrease in adipogenesis pathway (GSE2508). (c-e) Sirt1 significantly negative correlates with apoptosis pathway (c), sphingolipid pathway (d) and ceramide related pathway gene expression (e) in human adipose tissue (GSE2508). (f) Analysis of ceramide pathway genes expression in adipose stem cells (ASC) from subcutaneous WAT of morbidly obese and non-obese individuals. Human data set number is GSE48964.

signalling in the inguinal fat of *ATKO* mice (Fig. 7h). Consistently, more cleaved caspase 3 was observed in white adipose tissue from *ATKO* mice at 1 month of age (Fig. 7i), indicating that a higher level of apoptosis induced by ceramide is positively correlated with more adipogenesis. Collectively, these results indicate that ceramide accumulation during early adipogenesis is effectively regulated by Sirt1 upon epigenetic alteration, and this provides a potential target for obesity treatment.

4. Discussion

Adipose tissue is comprised of adipocytes at different stages of differentiation. Meanwhile, there is marked variation in the gene expression profiles of adipocytes at different stages of adipogenesis, suggesting that different hallmark mechanisms contribute to adipogenesis progression [47]. Although C/EBPα and PPARγ are well established factors regulating adipogenesis progression, they are very difficult to target with drugs. Metabolic characteristics integrate intrinsic gene expression and protein abundance with extrinsic environmental factors [10]. Modulating metabolism is capable of maintaining cell potency, determining cell fate into certain cell types [11−13]. However, little is known regarding the metabolic landscape during the switching of precursors into adipocytes. Dissecting which metabolic network is fundamental for early adipogenesis commitment can provide a potential target for obesity treatment.

Here, we depict an ongoing metabolic footprint during adipocyte commitment. Our results uncover a complex array of metabolism enriched as early as 3 h, which tend to fluctuate throughout differentiation. By 48 h of differentiation, the metabolic networked focused on ceramide production. Mechanistically, ceramide accumulation stemming from hydrolysis and the *de novo* pathway during early adipogenesis was effectively modulated by Sirt1 via epigenetic alterations, such as Histone H3K4 methylation and H3K9 acetylation.

The first biological consequence of ceramide accumulation during early adipogenesis is to induce apoptosis. Our results demonstrate that apoptosis is essential for adipogenesis. Studies have clearly
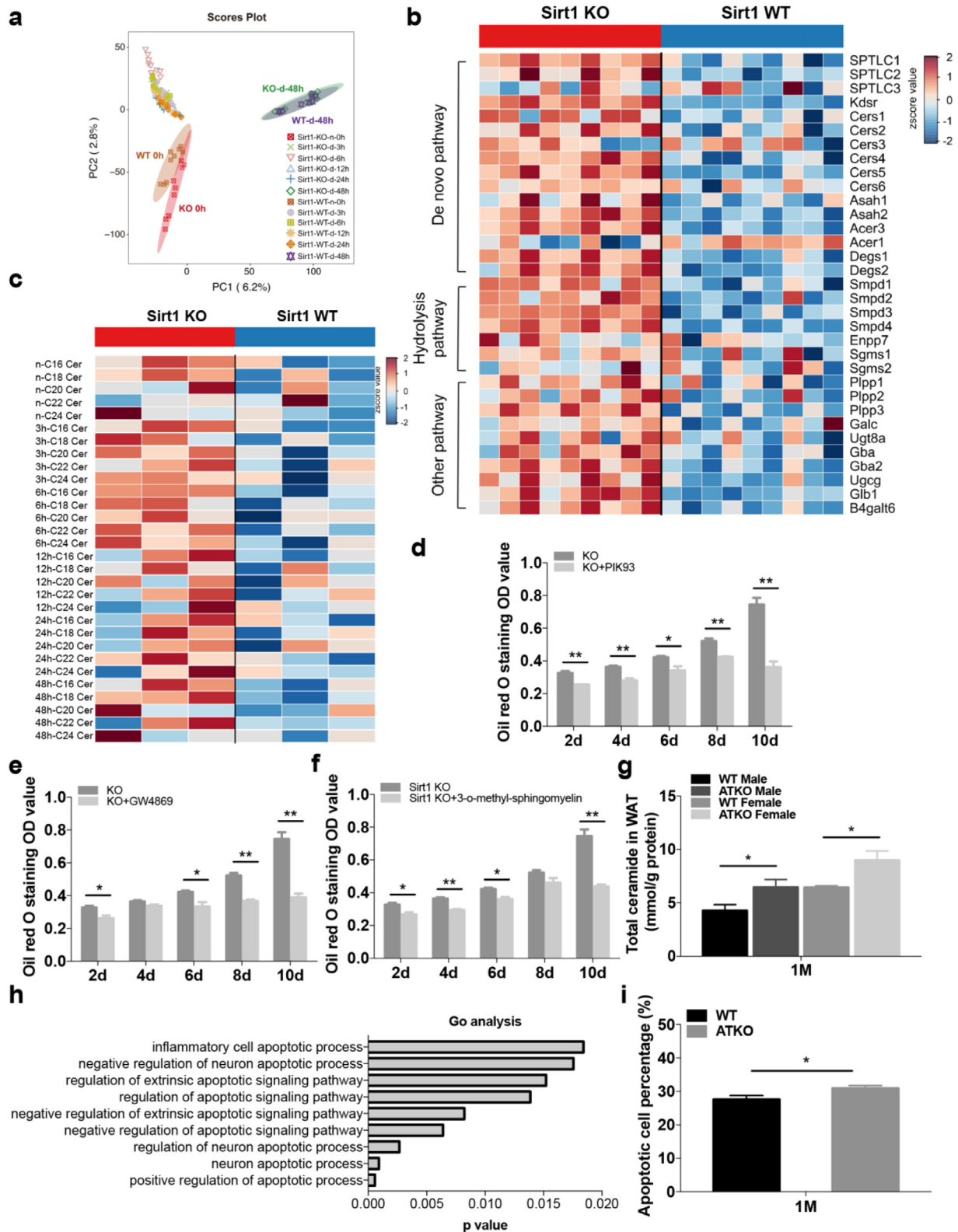
Fig. 7. Modulating ceramide levels by Sirt1 provides a potential target for obesity treatment. (a) PLS-DA analysis of *Sirt1* WT and *Sirt1* KO MEFs metabolites during early stage adipogenesis. (*n* = 9 for each group). (b) The expression of genes that are involved in ceramide production was analyzed by Q-PCR in *Sirt1* WT and *Sirt1* KO MEF cells (*n* = 9 for each group). (c) Different species of ceramide variation in *Sirt1* WT and *Sirt1* KO MEF cells during early stage adipogenesis. (*n* = 3 for each group) (d-f) Quantification of oil red O staining result of *Sirt1* KO MEFs by ceramide inhibitor PIK93 (d), GW4869 (e) and 3-O-Methyl-sphingomyelin (f) treatment after 24 h differentiation during adipogenesis (*n* = 3 for each group). (g) Ceramide content in white adipose tissue of *Sirt1* WT and *Sirt1* ATKO mice at 1-month ages (*n* = 6 for each group). (h) Pathway analysis of Exon array data from adipose tissues. (i) The apoptotic cell percentage in the inguinal fat tissues from *WT* and *ATKO* mice of 1-month old is quantified by IHC staining of cleaved Caspase 3 (*n* = 6 for each group). Results are expressed as mean±SEM. *Student's t-test* was used for the statistical analysis; **$p < 0.01$, *$p < 0.05$.

shown that apoptosis induced via caspase 3, 8, 9, 12, Bid, and Bax is present in rodent and human adipose tissue [48]. Although apoptosis has been observed both *in vivo* and *in vitro*, apoptosis was not considered an initiating process for adipogenesis; instead, the conventional concepts suggest that adipocytes die of apoptosis due to obesity, insulin resistance and hepatic steatosis [49,50].

Inhibition of apoptosis by inhibitors or acute RNAi-mediated loss of caspase 3 resulted in impaired adipogenesis. Moreover, the co-culture of 3T3-L1 cells with apoptotic cells increased adipogenesis. Indeed, we show that apoptotic cells self-decomposed to release fatty acids into the medium. Interestingly, the lipophilic content of apoptotic cell population promoted adipogenesis through upregulation of PPARγ and C/EBPα gene transcription. We did notice that this event only occurred 24 h post-incubation in differentiation medium, coinciding with the spike in ceramide content. We performed time-

course experiments in combination with inhibitor treatment to elucidate this time-dependent phenomenon. Our data support a dual role for ceramide in the adipogenesis model. The BTX components first induced ceramide content fluctuation in a certain cell population, and the altered ceramide content then pushed these cells towards apoptosis. The apoptotic cells then presented the lipid/ceramide to the non-apoptotic cell population to trigger adipogenesis and form lipid droplets. Fatty acid modulates enzymes of lipid metabolism to promote adipogenesis [30,31].

Obesity is characterized by increased adipose tissue mass, which is driven either by adipocyte hypertrophy (the increase of existing adipocyte size) or adipocyte hyperplasia (the increased number of new adipocytes from precursor differentiation in the process of adipogenesis) [7]. Clinical usage of FDA-approved drugs for obesity is limited by the pronounced side effects [9,51]. Our data suggest that
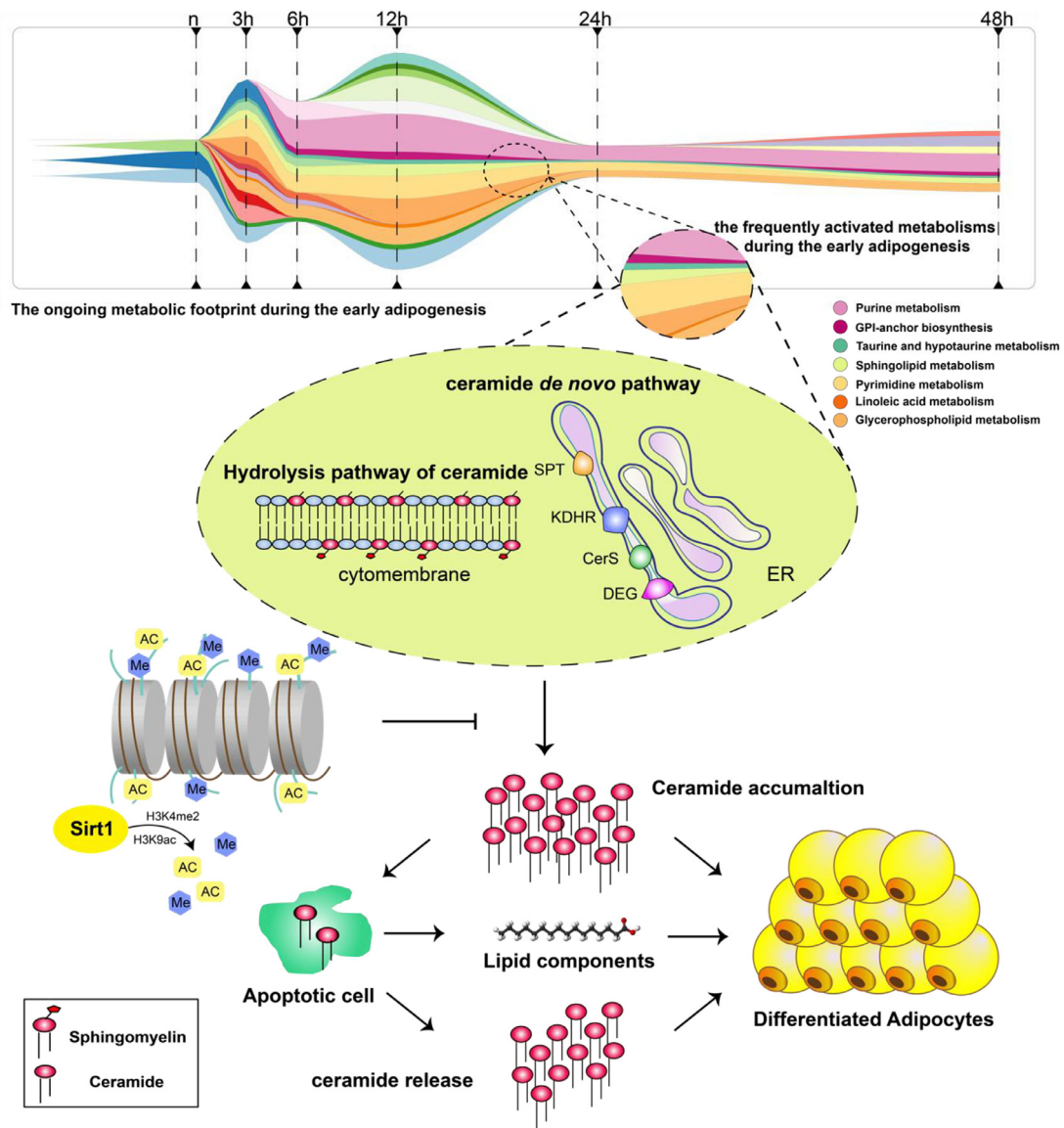

Fig. 8. The metabolic footprints during adipocyte commitment highlights ceramide metabolism as an adequate approach for obesity treatment. The metabolic footprint during adipocyte commitment depicted a complicated and diversified metabolic network, which was enriched as early as 3 h, and tended to fluctuate throughout differentiation time. Subsequently, the spectrum of these perturbed metabolic patterns was limited to some defined metabolic pathways, such as purine metabolism, GPI-anchor biosynthesis, taurine and hypotaurine metabolism, sphingolipid metabolism, pyrimidine metabolism, linoleic acid metabolism, and glycerophospholipid metabolism. These metabolic alterations reached to a relatively equipoised state at 48 h of differentiation. These frequently activated metabolisms were related to apoptosis. High relevance is the presence of apoptosis induced by ceramide accumulation, which associates with metabolic dynamics. Apoptotic cells were not merely as the byproduct of the adipogenesis process, but a promoting factor for releasing lipid components to facilitate adipogenesis. Mechanistically, ceramide accumulation stemming from hydrolysis and the de novo pathway during the early adipogenesis is effectively modulated by Sirt1 upon epigenetic alterations of constitutive Histone H3K4 methylation and H3K9 acetylation, which provides a potential target for obesity treatment.

targeting ceramide production can block new adipocyte generation, but there is no evidence that inhibiting adipocyte differentiate will lead to accumulated lipid droplets. Given that approximately 10% of adipocytes are renewed annually at all adult ages, targeting ceramide for anti-obesity may not lead to lipotoxicity [52,53]. Of note, a novel therapeutic approach to treat obesity by targeting adipocyte apoptosis has attracted public attention [54]. Our studies show the possible reversible effect by targeting adipocyte apoptosis or ceramide production for obesity treatment. Our findings might provide more meaningful candidates for druggable targets of obesity.

Ceramides differ in a carbon chain of fatty acid, in which the carbon number restricts its transportation in cellular organelles [55]. In mammals, the CerS family consists of 6 isoforms, which show substrate preference for sphinganine with a definite carbon chain of fatty acyl CoAs. These synthetic dihydroceramides are further desaturated by dihydroceramide desaturase to form ceramide [56,57]. Recently, growing evidence has shown that ceramide or ceramide metabolism is associated with a risk of metabolic syndrome, including cardiovascular disease, Alzheimer's disease, or diabetes [58−61]. Several studies have focused on ceramidases. Ceramidases remove an acyl-chain from ceramide to form sphingosine, which displays no similar function with ceramide for insulin pathway or apoptosis [62]. However, ceramide production is a very complicated metabolic process, including the de novo pathway in ER, hydrolysis pathway of sphingomyelin, and salvage pathway in the lysosome [55]. Of the six ceramide synthases, each favours relatively defined chain lengths of fatty acyl CoAs for different carbon chains of ceramides [63]. Meanwhile, the temporal-spatial profile of intermediate products of ceramide metabolism can interact or crosstalk to maintain homeostasis. Thus, targeting single or several genes of ceramide metabolism might lead to an unsuccessful result. Our studies show that Sirt1 regulates different carbon chains of ceramides from hydrolysis and the *de novo* pathway by affecting the expression of the enzymes involved via epigenetic regulation. This *in vitro* and *in vivo* experimental result provides a potential array of targets for obesity and ceramide-related metabolic syndromes.

In summary, we demonstrate that ceramide production fluctuates to induce apoptosis during adipogenesis. The apoptotic process is essential for initiating adipogenesis by providing lipophilic components to activate adipogenic transcription factor expression and facilitate lipid droplet formation. Sirt1 is involved in regulating ceramide production via epigenetically modifying the activity of related promoters (Fig. 8).

Declaration of Competing Interest

M.L.K.C. reports personal fees from Astellas, personal fees from Janssen, grants and personal fees from Ferring, non-financial support from Astrazeneca, personal fees and non-financial support from Varian, grants from Sanofi Canada, grants from GenomeDx Biosciences and non-financial support from Medlever, outside the submitted work. The other authors declare no competing interests.

Author contribution

Conceptualization, R.H.W., and W.L.H; Methodology, W.L.H., and Q.C.; Formal Analysis, W.L.H., H.T.W., Q.C., and R.H.W.; Investigation, W.L.H; Writing-Original Draft, W.L.H.; Writing-Review & Editing, R.H.W., C.X.D., Q.C., M.L.K., and Y.E.C.; Funding Acquisition, R.H.W., Q.C., and C.X.D.; Resources, R.H.W., Q.C., and C.X.D.; Supervision, C.X.D., and R.H.W

Supplementary materials

Supplementary material associated with this article can be found in the online version at doi:10.1016/j.ebiom.2019.102605.

References

[1] Molly Warren S, Stacy Beck J, Jack Rayburn M. The state of obesity: 2018. Robert Wood Johnson Foundation; 2018.
[2] Jensen MD, Ryan DH, Apovian CM, Ard JD, Comuzzie AG, Donato KA, et al. 2013 AHA/ACC/TOS guideline for the management of overweight and obesity in adults: a report of the American College of Cardiology/American Heart Association task force on practice guidelines and the Obesity Society. J Am College Cardio 2014;63 (25_PA).
[3] Duseja A, Singh SP, Saraswat VA, Acharya SK, Chawla YK, Chowdhury S, et al. Non-alcoholic fatty liver disease and metabolic syndrome—position paper of the Indian national association for the study of the liver, endocrine society of India, Indian College of Cardiology and Indian Society of Gastroenterology. J Clin Exp Hepatol 2015;5(1):51–68.
[4] Bruce K, Szczepankiewicz D, Sihota K, Ravindraanandan M, Hanson M, Byrne C, et al. Offspring of mothers on a high fat diet show altered circadian biology and fatty liver. In: Proceedings of The Physiological Society. The Physiological Society; 2013.
[5] Park J, Morley TS, Kim M, Clegg DJ, Scherer PE. Obesity and cancer—mechanisms underlying tumour progression and recurrence. Nat Rev Endocrinol 2014;10 (8):455.
[6] Berger NA. Obesity and cancer pathogenesis. Ann N Y Acad Sci 2014;1311:57.
[7] Ghaben AL, Scherer PE. Adipogenesis and metabolic health. Nat Rev Mol Cell Biol 2019;20(4):242–58.
[8] Arner E, Westermark PO, Spalding KL, Britton T, Rydén M, Frisén J, et al. Adipocyte turnover: relevance to human adipose tissue morphology. Diabetes 2010;59 (1):105–9.
[9] Kang JG, Park C-Y. Anti-obesity drugs: a review about their effects and safety. Diabetes Metab J 2012;36(1):13–25.
[10] Drehmer DL, de Aguiar AM, Brandt AP, Petiz L, Cadena SMSC, Rebelatto CK, et al. Metabolic switches during the first steps of adipogenic stem cells differentiation. Stem Cell Res 2016;17(2):413–21.
[11] Yanes O, Clark J, Wong DM, Patti GJ, Sánchez-Ruiz A, Benton HP, et al. Metabolic oxidation regulates embryonic stem cell differentiation. Nat Chem Biol 2010;6(6):411.
[12] Shiraki N, Shiraki Y, Tsuyama T, Obata F, Miura M, Nagae G, et al. Methionine metabolism regulates maintenance and differentiation of human pluripotent stem cells. Cell Metab 2014;19(5):780–94.
[13] Rafalski VA, Mancini E, Brunet A. Energy metabolism and energy-sensing pathways in mammalian embryonic and adult stem cell fate. J Cell Sci 2012;125 (23):5597–608.
[14] Ntambi JM, Young-Cheul K. Adipocyte differentiation and gene expression. J Nutr 2000;130(12):3122S–6S.
[15] Yabu T, Shiba H, Shibasaki Y, Nakanishi T, Imamura S, Touhata K, et al. Stress-induced ceramide generation and apoptosis via the phosphorylation and activation of nSMase1 by JNK signaling. Cell Death Differ 2015;22(2):258.
[16] Hannun YA, Obeid LM. Ceramide: an intracellular signal for apoptosis. Trends Biochem Sci 1995;20(2):73–7.
[17] Morad SA, Cabot MC. Ceramide-orchestrated signalling in cancer cells. Nat Rev Cancer 2013;13(1):51.
[18] Cho Y-W, Hong S, Jin Q, Wang L, Lee J-E, Gavrilova O, et al. Histone methylation regulator PTIP is required for PPARγ and C/EBPα expression and adipogenesis. Cell Metab 2009;10(1):27–39.
[19] Zebisch K, Voigt V, Wabitsch M, Brandsch M. Protocol for effective differentiation of 3T3-L1 cells to adipocytes. Anal Biochem 2012;425(1):88–90.
[20] Matsubara T, Tanaka N, Krausz KW, Manna SK, Kang DW, Anderson ER, et al. Metabolomics identifies an inflammatory cascade involved in dioxin-and diet-induced steatohepatitis. Cell Metab 2012;16(5):634–44.
[21] Yang Q, Wang B, Gao W, Huang S, Liu Z, Li W, et al. SIRT1 is downregulated in gastric cancer and leads to G1-phase arrest via NF-κB/Cyclin D1 signaling. Mol Cancer Res 2013;11(12):1497–507.

[22] Inaba M, Buszczak M, Yamashita YM. Nanotubes mediate niche-stem-cell signalling in the Drosophila testis. Nature 2015;523(7560):329–32.

[23] Huang J, Duran A, Reina-Campos M, Valencia T, Castilla EA, Müller TD, et al. Adipocyte p62/SQSTM1 suppresses tumorigenesis through opposite regulations of metabolism in adipose tissue and tumor. Cancer Cell 2018;33(4):770–84 e6.

[24] Hu C, Fan L, Cen P, Chen E, Jiang Z, Li L. Energy metabolism plays a critical role in stem cell maintenance and differentiation. Int J Mol Sci 2016;17(2):253.

[25] Ito K, Suda T. Metabolic requirements for the maintenance of self-renewing stem cells. Nat Rev Mol Cell Biol 2014;15(4):243.

[26] Tang Q-Q, Otto TC, Lane MD. CCAAT/enhancer-binding protein β is required for mitotic clonal expansion during adipogenesis. Proc Natl Acad Sci 2003;100(3):850–5.

[27] Oishi Y, Manabe I, Tobe K, Tsushima K, Shindo T, Fujiu K, et al. Krüppel-like transcription factor KLF5 is a key regulator of adipocyte differentiation. Cell Metab 2005;1(1):27–39.

[28] Guo L, Li X, Tang Q-Q. Transcriptional regulation of adipocyte differentiation: a central role for CCAAT/enhancer-binding protein (C/EBP) β. J Biol Chem 2015;290(2):755–61.

[29] Suzanne M, Steller H. Shaping organisms with apoptosis. Cell Death Differ 2013;20(5):669.

[30] Unno Y, Yamamoto H, Takatsuki S, Sato Y, Kuranaga T, Yazawa K, et al. Palmitoyl lactic acid induces adipogenesis and a brown fat-like phenotype in 3T3-L1 preadipocytes. Biochimica et Biophysica Acta (BBA)-Molecular and Cell Biology of Lipids 2018;1863(7):772–82.

[31] Yu H, Li R, Huang H, Yao R, Shen S. Short−Chain fatty acids enhance the lipid accumulation of 3T3−L1 cells by modulating the expression of enzymes of fatty acid metabolism. Lipids 2018;53(1):77–84.

[32] Trajkovic K, Hsu C, Chiantia S, Rajendran L, Wenzel D, Wieland F, et al. Ceramide triggers budding of exosome vesicles into multivesicular endosomes. Science 2008;319(5867):1244–7.

[33] Kitatani K, Usui T, Sriraman SK, Toyoshima M, Ishibashi M, Shigeta S, et al. Ceramide limits phosphatidylinositol-3-kinase C2β-controlled cell motility in ovarian cancer: potential of ceramide as a metastasis-suppressor lipid. Oncogene 2016;35(21):2801.

[34] Sprott KM, Chumley MJ, Hanson JM, Dobrowsky RT. Decreased activity and enhanced nuclear export of CCAAT-enhancer-binding protein β during inhibition of adipogenesis by ceramide. Biochem J 2002;365(1):181–91.

[35] Morad SAF, Cabot MC. Ceramide-orchestrated signalling in cancer cells. Nat Rev Cancer 2012;13:51.

[36] Tóth B, Balla A, Ma H, Knight ZA, Shokat KM, Balla T. Phosphatidylinositol 4-kinase IIIβ regulates the transport of ceramide between the endoplasmic reticulum and Golgi. J Biol Chem 2006.

[37] Mondal S, Mandal C, Sangwan R, Chandra S, Mandal C. Withanolide D induces apoptosis in leukemia by targeting the activation of neutral sphingomyelinase-ceramide cascade mediated by synergistic activation of c-Jun N-terminal kinase and p38 mitogen-activated protein kinase. Mol Cancer 2010;9(1):239.

[38] Chen S, Lee JM, Zeng C, Chen H, Hsu CY, Xu J. Amyloid beta peptide increases DP5 expression via activation of neutral sphingomyelinase and JNK in oligodendrocytes. J Neurochem 2006;97(3):631–40.

[39] Martin SF, Williams N, Chatterjee S. Lactosylceramide is required in apoptosis induced by N-Smase. Glycoconj J 2006;23(3−4):147–57.

[40] Aguilar-Arnal L, Katada S, Orozco-Solis R, Sassone-Corsi P. NAD+-SIRT1 control of H3K4 trimethylation through circadian deacetylation of MLL1. Nat Struct Mol Biol 2015;22:312.

[41] Wang QA, Tao C, Gupta RK, Scherer PE. Tracking adipogenesis during white adipose tissue development, expansion and regeneration. Nat Med 2013;19(10):1338–44.

[42] Wilhelm F, Hirrlinger J. Multifunctional roles of NAD+ and nadh in astrocytes. Neurochem Res 2012;37(11):2317–25.

[43] Walker MA, Tian R. NAD (H) in mitochondrial energy transduction: implications for health and disease. Curr Opin Physiol 2018.

[44] Picard F, Kurtev M, Chung N, Topark-Ngarm A, Senawong T, De Oliveira RM, et al. Sirt1 promotes fat mobilization in white adipocytes by repressing PPAR-γ. Nature 2004;429(6993):771.

[45] Jin Q, Zhang F, Yan T, Liu Z, Wang C, Ge X, et al. C/EBPα regulates SIRT1 expression during adipogenesis. Cell Res. 2010;20(4):470.

[46] Han L, Zhou R, Niu J, McNutt MA, Wang P, Tong T. SIRT1 is regulated by a PPARγ−SIRT1 negative feedback loop associated with senescence. Nucleic Acids Res 2010;38(21):7458–71.

[47] Richard AJ, Stephens JM. Emerging roles of JAK−STAT signaling pathways in adipocytes. Trend Endocrinol Metabol 2011;22(8):325–32.

[48] Herold C, Rennekampff HO, Engeli S. Apoptotic pathways in adipose tissue. Apoptosis 2013;18(8):911–6.

[49] Sorisky A, Magun R, Gagnon A. Adipose cell apoptosis: death in the energy depot. Int J Obes 2000;24(S4):S3.

[50] Alkhouri N, Gornicka A, Berk MP, Thapaliya S, Dixon LJ, Kashyap S, et al. Adipocyte apoptosis, a link between obesity, insulin resistance, and hepatic steatosis. J Biol Chem 2010;285(5):3428–38.

[51] Padwal RS, Majumdar SR. Drug treatments for obesity: orlistat, sibutramine, and rimonabant. Lancet North Am Ed 2007;369(9555):71–7.

[52] Spalding KL, Arner E, Westermark PO, Bernard S, Buchholz BA, Bergmann O, et al. Dynamics of fat cell turnover in humans. Nature 2008;453:783.

[53] Wang QA, Tao C, Gupta RK, Scherer PE. Tracking adipogenesis during white adipose tissue development, expansion and regeneration. Nat Med 2013;19:1338.

[54] Zhang Y, Huang C. Targeting adipocyte apoptosis: a novel strategy for obesity therapy. Biochem Biophys Res Commun 2012;417(1):1–4.

[55] Kihara A. Very long-chain fatty acids: elongation, physiology and related disorders. J Biochem 2012;152(5):387–95.

[56] Merrill AH. De novo sphingolipid biosynthesis: a necessary, but dangerous, pathway. J Biol Chem 2002;277(29):25843–6.

[57] Pewzner-Jung Y, Ben-Dor S, Futerman AH. When do Lasses (longevity assurance genes) become CerS (ceramide synthases)? Insights into the regulation of ceramide synthesis. J Biol Chem 2006;281(35):25001–5.

[58] Yuyama K, Mitsutake S, Igarashi Y. Pathological roles of ceramide and its metabolites in metabolic syndrome and Alzheimer's disease. Biochimica et Biophysica Acta (BBA)-Molecular and Cell Biology of Lipids 2014;1841(5):793–8.

[59] Teichgräber V, Ulrich M, Endlich N, Riethmüller J, Wilker B, De Oliveira−Munding CC, et al. Ceramide accumulation mediates inflammation, cell death and infection susceptibility in cystic fibrosis. Nat Med 2008;14(4):382.

[60] Li X, Becker KA, Zhang Y. Ceramide in redox signaling and cardiovascular diseases. Cell Physiol Biochem 2010;26(1):41–8.

[61] Haus JM, Kashyap SR, Kasumov T, Zhang R, Kelly KR, DeFronzo RA, et al. Plasma ceramides are elevated in obese subjects with type 2 diabetes and correlate with the severity of insulin resistance. Diabetes 2009;58(2):337–43.

[62] Summers SA. The ART of lowering ceramides. Cell Metab 2015;22(2):195–6.

[63] Cha HJ, He C, Zhao H, Dong Y, An I-S, An S. Intercellular and intracellular functions of ceramides and their metabolites in skin. Int J Mol Med 2016;38(1):16–22.